

2016

# Developing the framework for a risk map for mite vectored viruses in wheat resulting from pre-harvest hail damage

Anthony L. Nguy-Robertson  
*University of Nebraska-Lincoln*

Arthur Zygielbaum  
*University of Nebraska-Lincoln, aiz@unl.edu*


Anthony J. McMechan  
*University of Nebraska-Lincoln, justin.mcmechan@gmail.com*

Gary L. Hein  
*University of Nebraska-Lincoln, ghein1@unl.edu*

Stephen N. Wegulo  
*University of Nebraska-Lincoln, swegulo2@unl.edu*

*See next page for additional authors*

Follow this and additional works at: <http://digitalcommons.unl.edu/plantpathpapers>

 Part of the [Other Earth Sciences Commons](#), [Other Environmental Sciences Commons](#), [Other Plant Sciences Commons](#), [Plant Biology Commons](#), and the [Plant Pathology Commons](#)

---

Nguy-Robertson, Anthony L.; Zygielbaum, Arthur; McMechan, Anthony J.; Hein, Gary L.; Wegulo, Stephen N.; Stilwell, Abby R.; and Smith, Travis M., "Developing the framework for a risk map for mite vectored viruses in wheat resulting from pre-harvest hail damage" (2016). *Papers in Plant Pathology*. 377.  
<http://digitalcommons.unl.edu/plantpathpapers/377>

This Article is brought to you for free and open access by the Plant Pathology Department at DigitalCommons@University of Nebraska - Lincoln. It has been accepted for inclusion in Papers in Plant Pathology by an authorized administrator of DigitalCommons@University of Nebraska - Lincoln.

---

**Authors**

Anthony L. Nguy-Robertson, Arthur Zygielbaum, Anthony J. McMechan, Gary L. Hein, Stephen N. Wegulo, Abby R. Stilwell, and Travis M. Smith



## Developing the framework for a risk map for mite vectored viruses in wheat resulting from pre-harvest hail damage



Anthony L. Nguy-Robertson <sup>a,\*</sup>, Arthur I. Zygielbaum <sup>a</sup>, Anthony J. McMechan <sup>b</sup>, Gary L. Hein <sup>b</sup>, Stephen N. Wegulo <sup>c</sup>, Abby R. Stilwell <sup>a</sup>, Travis M. Smith <sup>d,e</sup>

<sup>a</sup> Center for Advanced Land Management Information Technologies, School of Natural Resources, University of Nebraska-Lincoln, Lincoln, NE, USA

<sup>b</sup> Department of Entomology, University of Nebraska-Lincoln, Lincoln, NE, USA

<sup>c</sup> Department of Plant Pathology, University of Nebraska-Lincoln, Lincoln, NE, USA

<sup>d</sup> Cooperative Institute of Mesoscale Meteorological Studies, University of Oklahoma, Norman, OK, USA

<sup>e</sup> National Severe Storms Laboratory, National Oceanic and Atmospheric Administration, Norman, OK, USA

### ARTICLE INFO

#### Article history:

Received 25 March 2016

Received in revised form

3 June 2016

Accepted 19 June 2016

#### Keywords:

Remote sensing

Landsat

MODIS

NOAA hail product

Nebraska

### ABSTRACT

There is a strong economic incentive to reduce mite-vectored virus outbreaks. Most outbreaks in the central High Plains of the United States occur in the presence of volunteer wheat that emerges before harvest as a result of hail storms. This study provides a conceptual framework for developing a risk map for wheat diseases caused by mite-vectored viruses based on pre-harvest hail events. Traditional methods that use NDVI were found to be unsuitable due to low chlorophyll content in wheat at harvest. Site-level hyperspectral reflectance from mechanically hailed wheat showed increased canopy albedo. Therefore, any increase in NIR combined with large increases in red reflectance near harvest can be used to assign some level of risk. The regional model presented in this study utilized Landsat TM/ETM+ data and MODIS imagery to help gap-fill missing data. NOAA hail maps that estimate hail size were used to refine the area most likely at risk. The date range for each year was shifted to account for annual variations in crop phenology based on USDA Agriculture statistics for percent harvest of wheat. Between 2003 and 2013, there was a moderate trend ( $R^2 = 0.72$ ) between the county-level insurance claims for Cheyenne County, Nebraska and the area determined to be at risk by the model (excluding the NOAA hail size product due to limited availability) when years with low hail claims (<400 ha) were excluded. These results demonstrate the potential of an operational risk map for mite-vectored viruses due to pre-season hail events.

This document is a U.S. government work and is not subject to copyright in the United States.

© 2016 Elsevier Ltd. All rights reserved.

### 1. Introduction

Wheat (*Triticum aestivum* L.) is a major economic crop in Nebraska ranking fifth in terms of cash receipts (Nebraska Department of Agriculture, 2012) and third in volume exported (Van Meter et al., 2012). Thus, there is a strong economic incentive to minimize loss due to diseases. Economically important diseases of wheat include those caused by viruses transmitted by the wheat curl mite (WCM, *Aceria tosichella* Keifer). These viruses are wheat streak mosaic virus (WSMV; Slykhuus, 1955), Triticum mosaic virus (TriMV; Seifers et al., 2009; Tatineni et al., 2009), and Wheat mosaic virus (WMoV; Seifers et al., 2007). Surveys of wheat fields in the

Great Plains of the United States determined WSMV to be the most prevalent of the three viruses (Burrows et al., 2009; Byamukama et al., 2013). Single, double, or triple infections of wheat by the viruses were confirmed, with a high frequency (91%) of co-infection with WSMV and TriMV (Burrows et al., 2009; Byamukama et al., 2013). Co-infection of wheat by WSMV and TriMV has been shown to decrease yield by 81–96% (Byamukama et al., 2014).

WCM-transmitted viruses are commonly found throughout the Great Plains of North America (Burrows et al., 2009), and the viruses have recently spread outside of North America (Schubert et al., 2015; Ellis et al., 2003; Truol et al., 2004). However, the highest risk for WSMV/TriMV outbreaks is volunteer wheat that emerges before harvest as a result of hail storms. The WCM has a short life cycle (egg to adult in 7–10 days) and cannot survive for more than a few days off green plants (Wosula et al., 2015). Volunteer wheat acts as a “green bridge” host for the WCM and

\* Corresponding author. 3310 Holdrege, Lincoln, NE, 68583-0973, USA.

E-mail address: [anthony.robertson@huskers.unl.edu](mailto:anthony.robertson@huskers.unl.edu) (A.L. Nguy-Robertson).

viruses between summer harvest and winter wheat planting in the fall (Gibson and Painter, 1956; Shahwan and Hill, 1984). If the volunteer wheat survives until planting, WCMs disperse, aided by wind or air currents, to the emerged winter wheat crop and transmit the viruses (Somsen and Sill, 1970). Controlling volunteer wheat through herbicide application or tillage before emergence of the winter wheat crop minimizes the risk of virus infection (Thomas et al., 2004). Therefore, identification of areas where pre-harvest volunteer wheat is likely to occur due to hail damage will facilitate timely control of volunteer wheat.

Hail damage has been successfully identified in different agricultural settings by evaluating changes to the spectral properties of vegetation (Gallo et al., 2012; Parker et al., 2005; Zhao et al., 2012). Healthy vegetation has low reflectance in the visible range of the electromagnetic spectrum due to absorption by pigments such as chlorophyll, carotenoids, and anthocyanins. Low reflectance in the visible range is contrasted by high reflectance in the near-infrared (NIR) region due to scattering at the leaf cellular level and canopy structure (Gitelson, 2011). The normalized difference vegetation index (NDVI) measures the difference between canopy absorption and scattering (Tucker, 1979) and is very sensitive to changes in green (photosynthetically active) leaf area index (gLAI) values below  $3 \text{ m}^2 \text{ m}^{-2}$  (Viña et al., 2011). Hail damage alters crop canopy structure and reduces absorption by pigments, such as chlorophyll. NDVI has been used in many studies to detect hail swaths due to its sensitivity to these changes (Erickson et al., 2004; Kalb and Bentley, 2002; Molthan et al., 2013; Peters et al., 2000). However, many of these studies were done in the middle of the growing season when canopy chlorophyll is high. The period when wheat grain is most likely to germinate if dislodged from heads by hail occurs at the end of the growing season when NDVI is typically low. Therefore, an approach using changes in NDVI may not be suitable, and alternatives should be explored.

The goal of this study was to develop a framework for using remote sensing products to identify high risk areas for transmission of WCM-vectored viruses to fall-planted wheat in the Nebraska Panhandle. Such products will allow farmers to execute management strategies to minimize the risk of future WSMV outbreaks. The specific objectives were to 1) identify the spectral behavior of wheat impacted by hail, 2) select suitable raster-based data that can identify hail events and hail damage, and 3) develop a series of risk maps for Cheyenne County, Nebraska, U.S.A. between 2003 and 2013.

## 2. Materials and methods

### 2.1. Mechanically hailed plots

Rainfed 'Pronghorn' winter wheat was mechanically hailed using a hail simulator at the High Plains Ag Lab (41.23019N, 102.99962W) near Sidney, Nebraska, U.S.A. Treatments were arranged in a randomized complete block, split-plot design with eight replications. The main plot treatments were four different hail dates during the heading stages of wheat; middle milk (Zadoks 75), early dough (Zadoks 83), soft dough (Zadoks 85), and hard dough/ripe (Zadoks 87/91). Example photographs of the hailed plots are in Fig. 1. The split-plot treatments were uncaged and caged ( $2 \text{ m} \times 2 \text{ m}$ ) to represent rapid and slow drying conditions, respectively, following the hail. Split-plot cages were placed one day after the hail treatment and removed seven days later. Plots were watered using a garden hose sprinkler with ca. 25 mm at 0, 2, and 4 days after hail application to simulate the expected rainfall accompanying a hail event.

Hail treatments were applied with a hail simulator attached to and powered by a tractor. For each plot, five 9 kg ice bags were

placed in a hopper at the top of the machine and fed into a vertical feeder housing containing a rotating horizontal cylinder with spikes that crushed the ice into 4–5 cm pieces. Ice was then propelled from the machine at approximately  $80 \text{ km h}^{-1}$  through a 20-cm diameter hose powered by a hydraulic air seeder fan. The hose was directed toward the wheat across the entire plot ( $2 \text{ m} \times 2 \text{ m}$ ) in a continuous motion at a 45-degree angle for uniformity between plots.

The spectral behavior of each plot was recorded one day prior to the hail application and at 1, 7 and 14 days after hail application. An adjacent field that did not have split-plot cages was used for reflectance measurements at harvest. Spectral behavior was recorded using a dual fiber system containing two USB2000 radiometers (Ocean Optics Inc. Dunedin, FL, U.S.A.). These radiometers have a sampling range of 400–900 nm, an interval of 0.3 nm, and a spectral resolution of 1.5 nm. The upwelling fiber had a  $25^\circ$  field of view and was held 1 m above the top of the canopy. This provided an area with a diameter of approximately 0.44 m. The downwelling fiber was equipped with a cosine corrector to measure incoming irradiance. The two radiometers were inter-calibrated using a white Spectralon panel (Labshere, Inc., North Sutton, NH, U.S.A.). The fibers were attached to a painter's pole to minimize the influence of the user on the reflectance and the pole was stabilized using a tripod. For more details on the radiometer system see Rundquist et al. (2004). Each reflectance reading was an average of eight scans collected over eight random positions over each plot. The plot level reflectance was an average of these readings over both caged and uncaged plots ( $n = 128$ ). Since the plots had not been divided yet, there were fewer reflectance readings at the start of the experiment ( $n = 64$ ). Similarly, there was an increased number of reflectance observations at harvest ( $n = 296$ ) to fully characterize the variability of the adjacent field. The median reflectance from each of the split-plot treatments was used to determine the plot-level reflectance. For statistical summaries, the hyperspectral reflectance was used to simulate the Landsat 8 spectral response curve where the standard error (SE) and coefficient of variation (CV) were calculated using Excel (v. 2013, Microsoft Corporation, Redmond, WA, U.S.A.) and the analysis of variance (ANOVA) between treatments was determined using R (v. 3.2.2 R Development Core Team, 2015). The fixed effect for the ANOVA tests was hail treatment and heading stage was a random effect.

### 2.2. Raster inputs for the risk model

Three remotely sensed products were utilized for this study: a NOAA hail size estimation product, Landsat Surface Reflectance from the Climate Data Record (CDR), and Moderate-resolution Imaging Spectroradiometer (MODIS) surface reflectance. In general, the NOAA hail size product provides information about the presence of hail in an area and the reflectance products identify changes in albedo and the details of the model are outlined in Fig. 2. The NOAA hail product is an optimal candidate for inclusion in the model. This product is created by blending remotely sensed three dimensional storm intensity data from multiple WSR-88D radars covering the area of interest with the vertical atmospheric temperature profile (Lakshmanan et al., 2007; Smith and Lakshmanan, 2011). This provides an estimate of maximal hail size aloft in a thunderstorm, with a horizontal resolution of  $0.01^\circ$  longitude by  $0.01^\circ$  latitude (approximately  $1 \text{ km}^2$ ). Although the product is intended for diagnosis of hail size aloft, Ortega et al. (2009) showed a strong relationship between predicted and measured hail size. The NOAA hail product is produced every two minutes; however, this resolution is much more frequent than necessary for seasonal use. One product representing maximal hail size over the period of highest risk should be sufficient for the model.

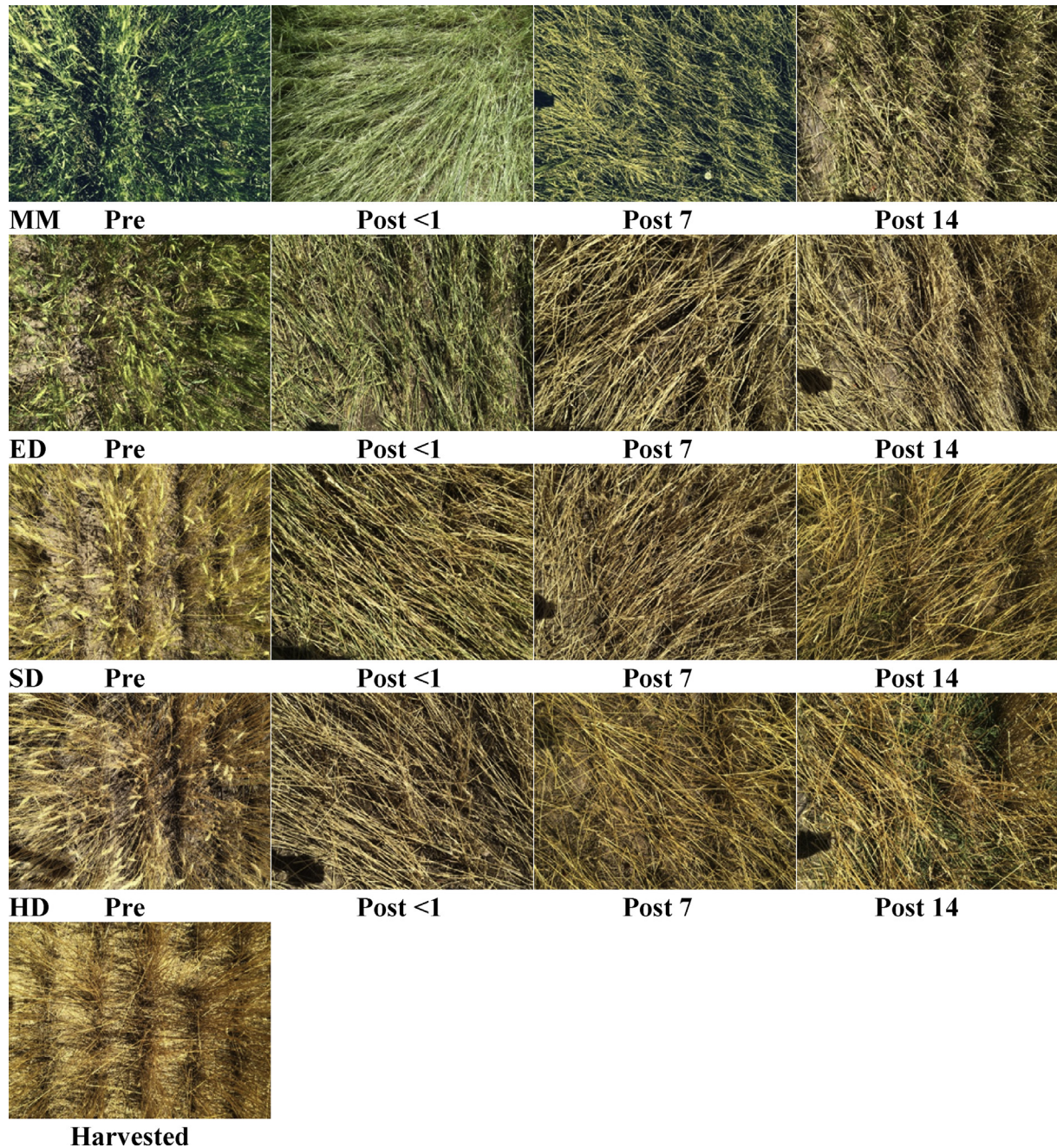


**Fig. 1.** Representative digital photos taken at nadir for the phenological stages of middle milk (MM), early dough (ED), soft dough (SD), and hard dough (HD) of the mechanically hailed sites for healthy wheat and wheat <1, 7, and 14 days post-hail. Healthy wheat after harvest is provided for reference. Volunteer wheat can be identified in the HD post 14 days.

Developing wheat grains are capable of germinating before maturity (Gosling et al., 1981; Robertson and Curtis, 1967); therefore, a hail event that occurs any time after wheat flowering, but before harvest, would increase the risk of producing volunteer wheat. The date when wheat reaches maturity varies each year, but the United States Department of Agriculture (USDA) publishes a crop progress report that includes the percentage of wheat harvested by date, which can be used to estimate the period between flowering and harvest. For the product presented below, we used the period starting three weeks (21 days) before 50% of wheat was harvested and ending when 90% of wheat had been harvested as reported for Nebraska, U.S.A. This encompasses a mean period of

$31.8 \pm 2.1$  (SD) days for the study area between 2003 and 2013 (Table 1). This period may need to be adjusted when applied to other locations as rates of crop maturity vary regionally.

There are several surface reflectance products available that have a variety of benefits and limitations based on spatial and temporal resolution. MODIS has an excellent temporal resolution (daily and 8-day composites); however, the spatial resolution is quite low (250, 500, or 1000 m depending on the spectral band). Conversely, the Thermal Mapper (TM), Enhanced Thermal Mapper Plus (ETM+), and Operational Land Imager (OLI) sensors aboard the Landsat series of satellites have higher spatial resolution (30 m) but are limited by the reduced revisit time (ca. 16 days). When cloud

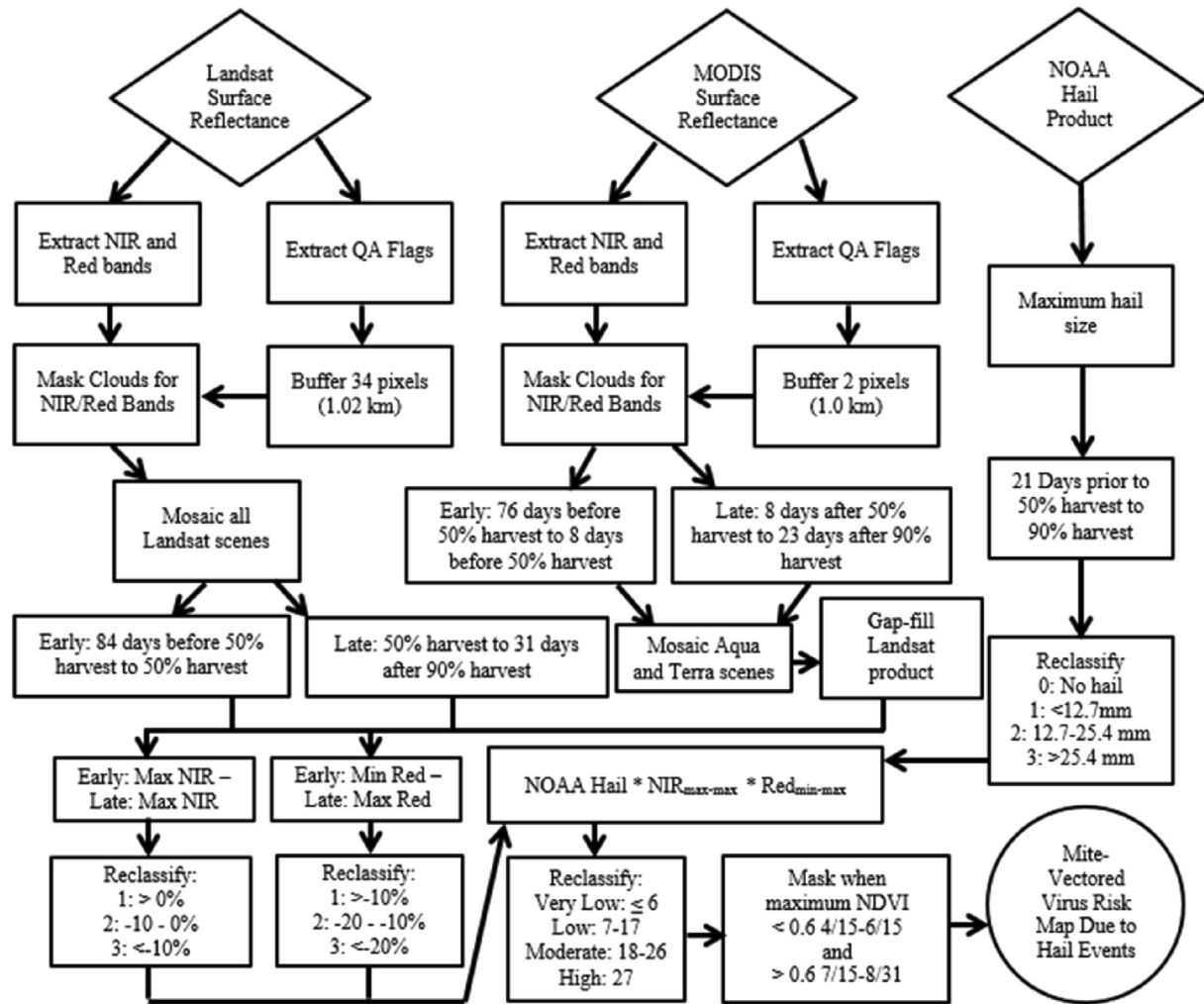


Fig. 2. Flowchart for the development of the mite-vector virus risk product from hail events.

Table 1

Start and end dates (Julian day) for raster integration based on USDA harvest reports.

Year	NOAA		Landsat				MODIS			
	Start	End	Early reflectance		Late reflectance		Early reflectance		Late reflectance	
			Start	End	Start	End	Start	End	Start	End
2003	173	204	110	173	173	235	118	165	181	227
2004	173	204	110	173	173	235	118	165	181	227
2005	169	203	106	169	169	234	114	161	177	226
2006	162	195	99	162	162	226	107	154	170	218
2007	170	201	107	170	170	232	115	162	178	224
2008	179	209	116	179	179	240	124	171	187	232
2009	177	210	114	177	177	241	122	169	185	233
2010	179	210	116	179	179	241	124	171	187	233
2011	181	213	118	181	181	244	126	173	189	236
2012	158	186	95	158	158	217	103	150	166	209
2013	180	213	117	180	180	244	125	172	188	236

cover and data gaps caused by the scan line corrector error for Landsat 7 are accounted for, the gap between image acquisitions can be quite large for some regions. Gaps can be filled using adjacent data (Maxwell et al., 2007), but this approach may not be ideal due to the potentially limited spatial extent of a hail event.

A combination of both MODIS and Landsat images can be used

to provide adequate spatial and temporal coverage of the region of interest. Surface reflectance products developed for both MODIS (Vermote and Kotchenova, 2011) and Landsat (Masek et al., 2006) have been shown to be consistent with ground-based measurements (Maiersperger et al., 2013). Landsat 5 (LT) imagery was used for this study; however after satellite failure, subsequent maps were developed using Landsat 7 (LE). Landsat 8 imagery could be used, but it was not explored as this product was not available at the time of the study.

There are four, 8-day composites composed of MODIS surface reflectance (09) available, which are based on either the Aqua (MYD) or Terra (MOD) sensor at a 250 (Q1) or 500 m (A1) spatial resolution. The CDR and MODIS surface reflectance products were accessed as \*.HDF files through EarthExplorer. All remaining processing steps were conducted in ArcGIS (v. 10.2, ESRI, Inc.) using python's integrated development environment, IDLE, (v. 2.7.3 Python Software Foundation). Due to limitations in the IDLE environment, the \*.HDF files were converted to GeoTIFFs.

Bands 3, 4 and 17, corresponding to red, NIR and flags, were extracted from the of the Landsat CDR product. While other bands in the visible range (e.g. green) may be more useful for identifying hail damage in immature wheat, the red band is frequently available from satellite sensors at better spatial resolutions (e.g. MODIS 250 m). A 1.02 km (34 pixel) buffer was placed around the cloud, cloud shadow, and snow flagged pixels (band 17) since pixels

surrounding clouds can also be impacted (Irish et al., 2006). This buffer was then used to remove these contaminated pixels from the red and NIR reflectance bands. All Landsat scenes acquired on the same day were mosaicked together. A similar pre-processing approach was used for MODIS surface reflectance products. The quality control flags are band 12 in the 500 m surface reflectance products (MOD09A1 and MYD09A1). Pixels that were flagged as cloud-contaminated were buffered by 1.0 km (2 pixels) and removed from the red and NIR reflectance bands in the 250 m surface reflectance products (MOD09Q1 and MYD09Q1).

### 2.3. Gap-filling approaches

Gap-filling methods using the same scene information, such as those used to fill in missing data from cloud covered pixels and gaps in the Landsat 7 data after the scan-line correction failure, introduce errors because of assumptions in interpolation (Maxwell et al., 2007; Zhang et al., 2007). In order to reduce gaps between Landsat scenes, we used a different approach that relies on measured data rather than interpolation. The minimum values of red and the maximum values of NIR reflectance for a given year were identified for all imagery between 84 days before 50% harvest to when 50% of wheat was harvested (Table 1). Imagery collected during this period was defined as “early” imagery. This period represents healthy wheat prior to harvest and/or hail damage. The maximum red and NIR reflectance between when 50% of wheat had been harvested and 31 days after 90% of wheat had been harvested (Table 1) represents senescing wheat, harvested wheat fields, and fields impacted by hail. The imagery collected during this period was defined as “late” imagery. Since hail damage causes increases in both red and NIR reflectance, differences between “early” and “late” products provide a change in reflectance that can be used to identify wheat damaged by hail. This approach should maintain small differences in reflectance due to hail damage, although sensitivity to these differences may be reduced as true maximum and minimum values may not be captured in the acquired imagery.

Even with this approach there are data gaps in the Landsat imagery. To accommodate these regions we utilized a similar approach using MODIS surface reflectance products. Since the day of the 8-day composite is not the actual date of acquisition for a given pixel, we used a slightly narrower range of imagery excluding the 8-day composite at the start and end of each cycle based on the USDA percent harvest threshold described for Landsat. See Table 1 for the exact dates.

### 2.4. Risk model development

Too many thresholds may be confusing to end-users. Thus, we limited our study to four thresholds at each level. Very low risk was assigned a ‘0’, low risk a ‘1’, moderate ‘2’, and high ‘3’. The U.S. National Weather Service defines severe hail as being 25.4 mm (1”) or greater (Cavanaugh and Schultz, 2012); however, when winds are strong enough, crop damage can occur with much smaller hail sizes (Changnon, 1971; Sánchez et al., 1996; Schiesser and Backfile, 1990). Therefore, no measured hail was classified as ‘0’, hail less than 12.7 mm (0.5”) was classified as ‘1’, 12.7–25.4 mm as ‘2’, and any measured hail greater than 25.4 mm was classified as ‘3’, the highest risk level (Fig. 2).

Senescing wheat typically has a reduction in NIR; however, increases in NIR can be attributed to hail damage (see *Spectral behavior of mechanically hailed plots* for details regarding the impact of hail on the wheat spectral signature). Increases of 10% in NIR reflectance between the early and late imagery were classified as ‘3’ while any increase in NIR less than 10% was classified as ‘2’. Any decrease in NIR was classified as ‘1’. Hail damage increases red

reflectance; but, so do senescence and chlorophyll degradation. Therefore, an additional threshold was applied for reflectance in the red region. Increases in red reflectance over 20% were classified as ‘3’ while increases between 10 and 20% were classified as ‘2’. Increases in red reflectance that were less than 10% and any decreases in reflectance were classified as ‘1’ (Fig. 2).

The final risk map for the entire region of interest was created with the three reclassified risk inputs (hail size, NIR and red reflectance; Fig. 2). The output for the risk map results in potential values between 0 and 27, which can be reassigned to new risk thresholds. Very low risk was classified to values ‘≤ 6’, low risk to values ‘7–17’, moderate risk to values ‘18–26’, and high risk to the value ‘27’.

This product would be suitable to provide to wheat growers within the region of interest as they know which fields or adjacent fields were planted with wheat and were truly at risk. Because the entire region of interest contains other land cover uses other than wheat (e.g. urban, non-wheat crops, native vegetation), a land cover classification approach would reduce false positives. Most classification schemes require a large data set with many observations (i.e. high temporal resolution) to separate vegetation types and accurate classification in real-time is difficult (Bargiel and Herrmann, 2011; Starks et al., 2014). Although there have been recent developments in real-time classification, they have generally been broad and not ideal for separating individual crop types (Huth et al., 2012).

This study utilized a simple classification scheme to mask most of the non-wheat area during the study period. The approach used NDVI maps during the spring growing season of wheat (April 15th to June 15th), and during the summer (July 15th to August 31st). Maximum NDVI values from all available Landsat imagery during both time periods were calculated. Pixels in which NDVI was less than 0.6 in the spring or above 0.6 in the summer were deemed to be some vegetation type other than wheat and masked. One drawback to using such a simple classification is that there will be some misclassifications. For example, similar to wheat, perennial crops like alfalfa are typically green early in the spring and are harvested periodically during the growing season (Wardlow et al., 2007). This creates a cyclical pattern in NDVI that may cause inclusion of some alfalfa fields, which would over-estimate risk for the purpose of validating the model using county-wide hail claims.

The risk model was applied to Cheyenne County, NE (41.22°N 102.99°W). While much of western Nebraska is primarily pastureland, the majority of Cheyenne County produces either hard red or hard white winter wheat (Van Meter et al., 2012). While risk maps using just Landsat reflectance data could be produced as far back as the availability of Landsat surface reflectance products (i.e. 1982), this study focused on the time period when insurance data were available for comparison with risk maps: 2003 to 2013. The insurance data were provided by the USDA Risk Management Agency (RMA) and aggregated only at the county-level due to privacy concerns. Available information included county, crop, type of damage, date of loss, and acreage. For each year in the study, the acreage classified as hail damage in wheat was aggregated for Cheyenne County, Nebraska, U.S.A. during the time period determined to be at risk (i.e. NOAA columns; Table 1). This excludes hail damage to wheat prior to heading that would not be of interest for a WCM-vectored virus risk product.

## 3. Results and discussion

### 3.1. Spectral behavior of mechanically hailed plots

As was observed in other studies that attempted to identify hail damage in various crops (Jedlovec et al., 2006; Yuan et al., 2002), hail events decreased NDVI (Fig. 3; Table 2). However, NDVI was not

always sensitive to hail damage. For example, there was no significant change in NDVI (ANOVA:  $f$ -value = 0.08,  $p$ -value = 0.79,  $Df = 1/51$ , Table 3) when wheat was hailed at the early dough stage (pre-hail NDVI = 0.55 vs. post-hail NDVI = 0.54, Table 2). Thus, NDVI can be a poor indicator of hail damage by itself.

When wheat was hailed, both red and NIR reflectance increased at all growth stages examined (Table 2) and were significantly different from healthy wheat (ANOVA:  $f$ -values 16–127,  $p$ -values < 0.001,  $Df = 1/30$ , Table 3); however, for red reflectance at the soft dough stage this was only weakly significantly different from red reflectance at harvest (ANOVA:  $f$ -value = 4.6,  $p$ -value = 0.04,  $Df = 1/51$ , Table 3). This was not surprising as both the hail damage and crop senescence increase red reflectance. Red reflectance of hailed wheat remained distinguishable from background healthy wheat reflectance at the middle milk, early dough, and soft dough stages for at least seven days (Table 3). However within the seven to fourteen day window the hail signature for both red and NIR reflectance faded and became indistinguishable from reflectance of wheat at harvest (Fig. 3; Table 3). This indicates that many observations (i.e. high temporal resolution) are needed to identify the spectral signature of hail to senescing wheat. While the week long intervals conducted in this study match the rough timeframe of Landsat observations, it was not enough to determine with specificity the length of the spectral signature, nor determine

the factors that caused it to degrade.

Since this study only examined mechanically hailed wheat, it is possible that naturally hailed wheat reflectance may differ from these results. The change in the orientation of the stalks was likely the main contributor to increases in albedo as it is well known that changes in view angle impact spectral behavior (e.g. Jackson et al., 1990). Changes in albedo may be useful in identifying hail damage on a regional scale in situations when vegetation is senescing.

Alternatively to identifying hail damage, identifying volunteer wheat would be of value as WCM propagation is highest when volunteer wheat emerges before harvest. Wheat grain is capable of germinating into volunteer wheat at all four growth stages; however, the risk is rather low initially and increases as wheat matures (Gosling et al., 1981; Robertson and Curtis, 1967). For the study plots, volunteer wheat was only observed 14 days after hailing the hard dough/ripe plots (Fig. 1). The emergence of volunteer wheat only marginally increased NDVI (Table 2) with only a weakly significant difference from wheat at harvest (ANOVA:  $f$ -value = 6.8,  $p$ -value = 0.01,  $Df = 1/51$ ). Additionally, NDVI will be an unreliable indicator using moderate to coarse spatial (e.g. 30–500 m) imagery as volunteer wheat emergence tends to be localized. Thus, the best metrics using civil sensors will be to observe changes in albedo such as the one that was used in developing the risk model (see Risk model development for details).

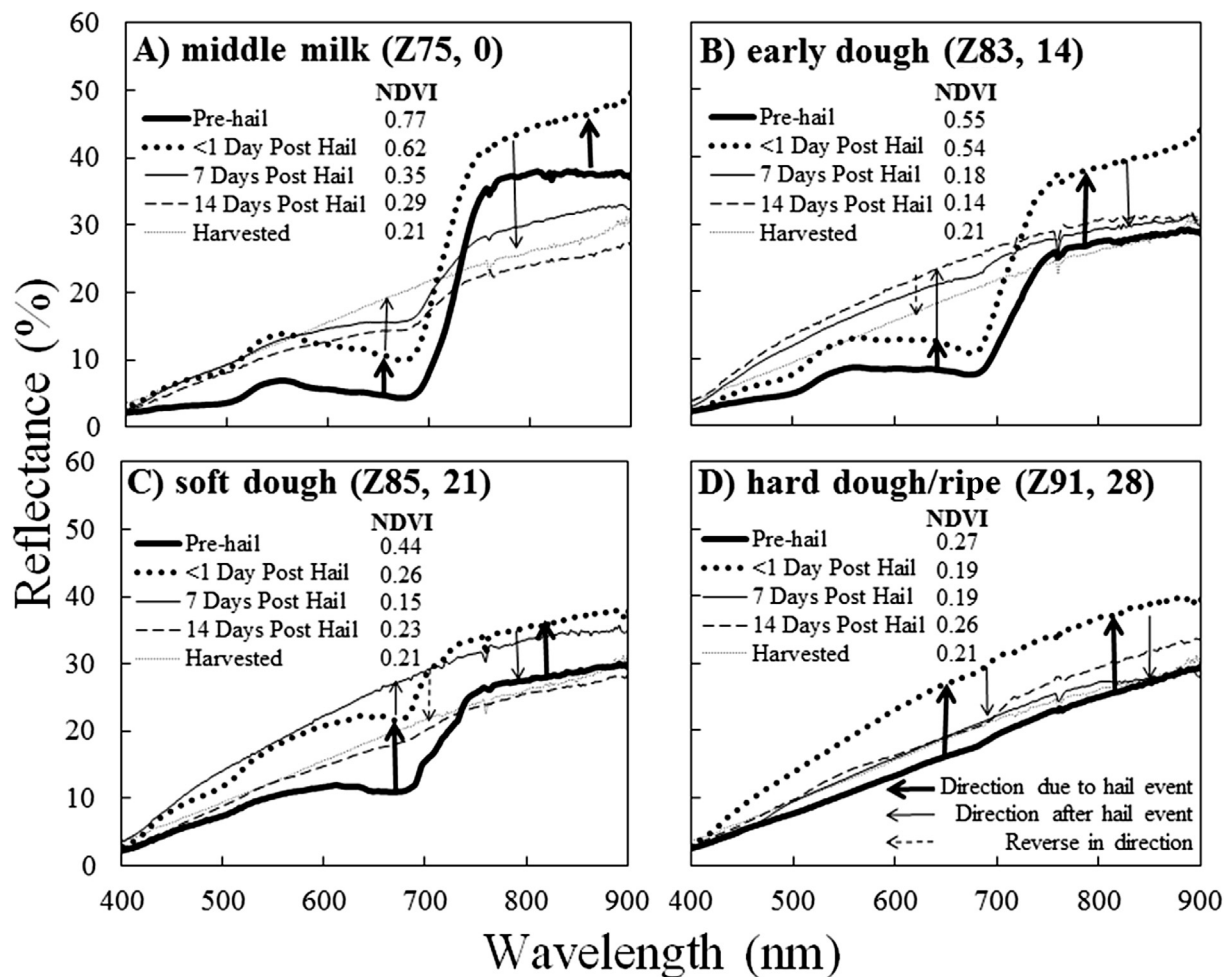


Fig. 3. Plot-level wheat reflectance collected prior to and after mechanical hail damage at four physiological stages of grain maturity (A) middle milk, (B) early dough, (C) soft dough, and (D) hard dough ripe. The Zadoks (Z) stage and days after reaching the middle milk stage at the hail event was indicated. Reflectance of harvested wheat and normalized difference vegetation index (NDVI) values are shown for reference.



**Table 2**

Variation in red and NIR reflectance and the normalized difference vegetation index (NDVI) collected over mechanically hailed wheat at different growth stages.

Crop stage	Days after hail	n	Red	SE	CV	NIR	SE	CV	NDVI	SE	CV
Middle milk	<sup>a</sup>	8	4.79	0.41	8.64	38.21	3.17	8.29	0.77	0.0188	2.43
	<1	16	11.49	2.09	18.17	45.61	5.39	11.82	0.60	0.0622	10.42
	7	16	17.28	3.82	22.09	31.00	3.59	11.58	0.29	0.0632	21.80
Early dough	14	16	14.38	1.75	12.19	24.90	1.58	6.36	0.29	0.0391	13.25
	<sup>a</sup>	16	8.04	0.83	10.35	27.81	1.97	7.07	0.55	0.0466	8.47
	0	16	11.30	1.84	16.32	38.35	5.63	14.67	0.54	0.0673	12.40
	7	16	21.83	2.57	11.77	36.84	2.61	7.08	0.17	0.0199	11.78
Soft dough	14	16	23.91	2.46	10.29	30.96	2.82	9.11	0.13	0.0161	12.44
	<sup>a</sup>	16	13.42	1.51	11.23	29.19	3.44	11.78	0.37	0.0468	12.68
	0	16	22.10	2.83	12.79	31.09	3.85	12.37	0.26	0.0601	23.34
	7	16	26.31	2.60	9.88	34.04	2.61	7.67	0.13	0.0159	12.36
Hard dough/ripe	14	16	18.06	0.50	11.17	26.50	0.49	7.35	0.19	0.0091	19.07
	<sup>a</sup>	16	17.64	2.52	14.28	27.82	3.78	13.60	0.27	0.0161	5.95
	0	16	27.69	3.02	10.91	37.45	3.79	10.11	0.15	0.0184	12.27
	7	16	20.04	0.55	10.88	27.10	0.67	9.85	0.15	0.0032	8.41
Harvest	14 <sup>b</sup>	16	18.86	4.72	15.90	30.08	7.52	10.57	0.27	0.0680	21.37
	<sup>a</sup>	37	18.77	0.93	30.20	27.11	1.08	24.23	0.19	0.0068	21.68

The sample size (n), standard error (SE), and coefficient of variation (CV) are reported.

<sup>a</sup> Spectra collected over non-hailed healthy wheat.<sup>b</sup> Increased standard error are for sites with volunteer wheat.**Table 3**ANOVA results between the red reflectance, near-infrared (NIR) reflectance and the normalized difference vegetation index (NDVI) of healthy wheat collected prior to being hailed, at harvest, or concurrently for those values collected pre-hail, <1, 7, and 14 days after being hailed. The fixed effect for the ANOVA tests was hail treatment and heading stage was a random effect. <sup>a</sup>No significant difference, all other values were significant at <sup>b</sup>90% or greater than 99% (no notation) levels of confidence. Bold indicates similarity between measurements. <sup>\*</sup>Indicates reflectance over healthy wheat was not collected for these dates.

Compared to healthy wheat:	Days after hail	Band or VI	Middle milk		Early dough		Soft dough		Hard dough/ripe	
			f-value	p-value	f-value	p-value	f-value	p-value	f-value	p-value
Prior to hail event	<1	Red	78.7	1.02E-8	41.2	4.39E-7	127	2.64E-12	106	2.32E-11
	<1	NIR	15.8	6.51E-4	51.4	5.61E-08	44.9	1.99E-7	44.9	2.02E-7
	<1	NDVI	57.3	1.45E-7	0.0752	<b>0.786<sup>a</sup></b>	35.9	1.42E-6	164	1.09E-13
	7	Red	83.9	5.83E-9	360	2.98E-18	292	5.33E-17	8.71	6.10E-3
	7	NIR	14.6	9.45 E-4	8.95	5.51E-3	16.3	3.45E-4	2.55	<b>0.120<sup>a</sup></b>
	7	NDVI	428	6.61E-16	896	6.64E-24	381	1.33E-18	300	3.66E-17
	14	Red	229	4.03E-13	592	2.63E-21	52.7	4.39E-8	1.70	<b>0.203<sup>a</sup></b>
	14	NIR	154	2.14E-11	11.2	2.26E-3	8.23	7.48E-3	2.76	<b>0.107<sup>a</sup></b>
	14	NDVI	1041	5.11E-20	1174	1.30E-25	150	3.39E-13	0.0361	<b>0.851<sup>a</sup></b>
	At harvest	<1	Red	23.9	1.04E-5	25.3	6.42E-6	4.63	<b>0.0361<sup>b</sup></b>	35.3
<1		NIR	95.5	2.81E-13	34.1	3.65E-7	30.8	1.02E-6	35.0	2.74E-7
<1		NDVI	581	1.57E-29	410	4.87E-26	10.9	1.77E-3	12.9	7.54E-4
7		Red	0.782	<b>0.381<sup>a</sup></b>	5.24	<b>0.0262<sup>b</sup></b>	26.4	4.47E-6	0.781	<b>0.381<sup>a</sup></b>
7		NIR	4.33	<b>0.0424<sup>b</sup></b>	3.49	<b>0.0676<sup>b</sup></b>	14.1	4.54E-4	0.245	<b>0.623<sup>a</sup></b>
7		NDVI	29.7	1.48E-6	8.30	5.79E-3	34.8	2.96E-7	19.1	6.02E-5
14		Red	8.67	4.87E-3	12.5	8.77 E-4	0.199	<b>0.657<sup>a</sup></b>	6.92E-3	<b>0.934<sup>a</sup></b>
14		NIR	2.42	<b>0.126<sup>a</sup></b>	3.00	<b>0.0891<sup>b</sup></b>	0.422	<b>0.519<sup>a</sup></b>	3.47	<b>0.0684<sup>b</sup></b>
14		NDVI	23.9	1.07E-5	38.9	8.67E-8	0.531	<b>0.469<sup>a</sup></b>	6.76	<b>0.0121<sup>b</sup></b>
Collected within one day		7	Red	*	*	116	8.00E-12	94.5	8.86E-11	*
	7	NIR	*	*	1.12	<b>0.297<sup>a</sup></b>	20.1	9.97E-5	*	*
	7	NDVI	*	*	262	2.30E-16	337	7.41E-18	*	*
	14	Red	170	6.82E-14	52.8	4.33E-8	*	*	*	*
	14	NIR	16.4	3.39E-4	2.37	<b>0.134<sup>a</sup></b>	*	*	*	*
	14	NDVI	314	1.92E-17	405	5.74E-19	*	*	*	*

### 3.2. Application of the risk model

The risk map (Fig. 4A) was a composite of the three inputs, the NOAA hail product (Fig. 4B), NIR (Fig. 4C) and red (Fig. 4D) reflectance based on the date ranges determined from USDA harvest reports (Table 1). While the range of dates for 50% harvest in Nebraska for the duration of the study was only 23 days, there was some variation. Harvest happened the soonest in 2012 and latest in 2011. This risk map was further processed to minimize the inclusion of land cover types other than wheat fields (Fig. 5). However, the NOAA hail product was still provisional and not available for all years in this study. For the purpose of comparing risk maps with hail claims (Fig. 6), only reflectance-based models

were used. The hail reports included in this comparison were limited to the period in which the NOAA hail product was integrated (Table 1) even though this product was not utilized in the model. For years when the area for hail claims was more than 400 ha, there was a moderate trend ( $R^2 = 0.72$ ) between the area where hail claims were received and the area determined to be at risk (Fig. 6B). When all years were included, this trend was not significant and extremely weak ( $R^2 < 0.01$ ). The model over-estimated when 'low risk' hail claim values were included. Ideally, field-level data would be used to validate this model; however, privacy concerns limit the access to these data. Adding the NOAA hail product may improve this relationship as relying entirely on the reflectance products will likely over-estimate

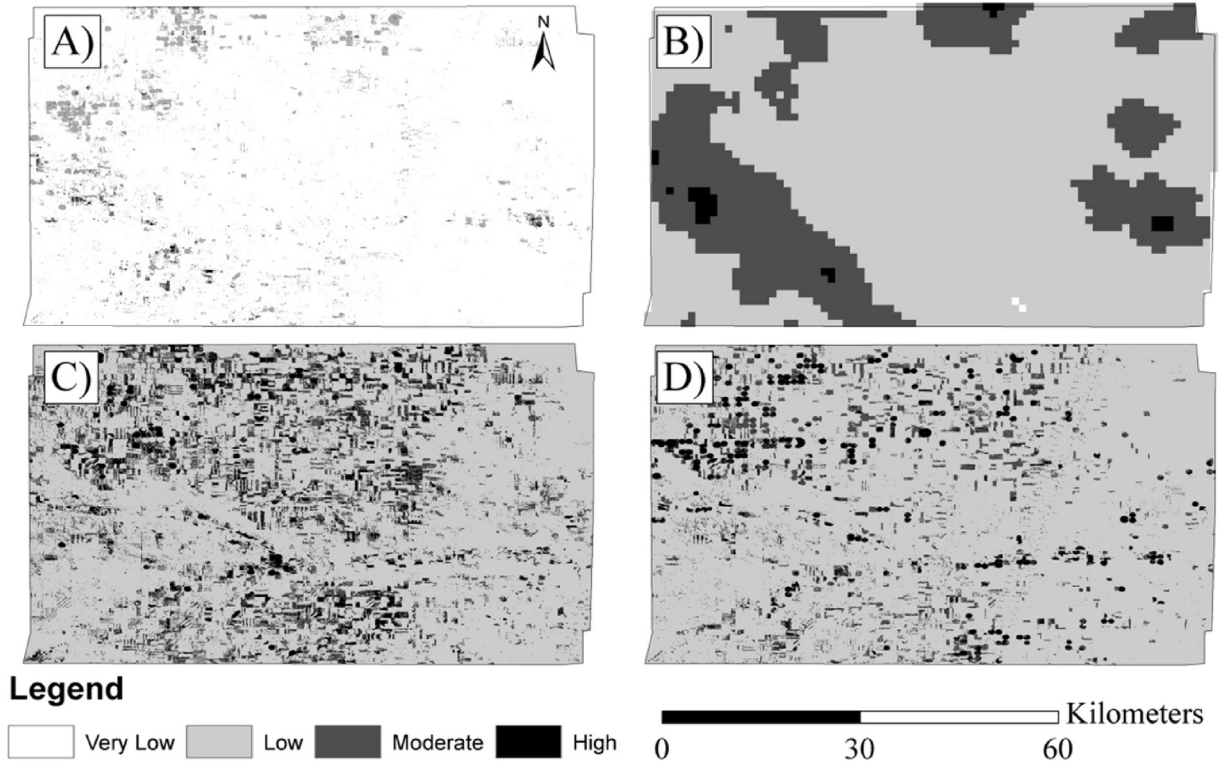


**Fig. 4.** The A) risk model for Cheyenne County, NE, U.S.A. in 2008 was based on three inputs: B) a radar-based maximal hail size during the period of highest risk for grain mature enough for volunteer wheat, C) the difference between maximal near infrared reflectance before and after harvest, and D) the difference between minimum red reflectance before harvest and maximum red reflectance after harvest.

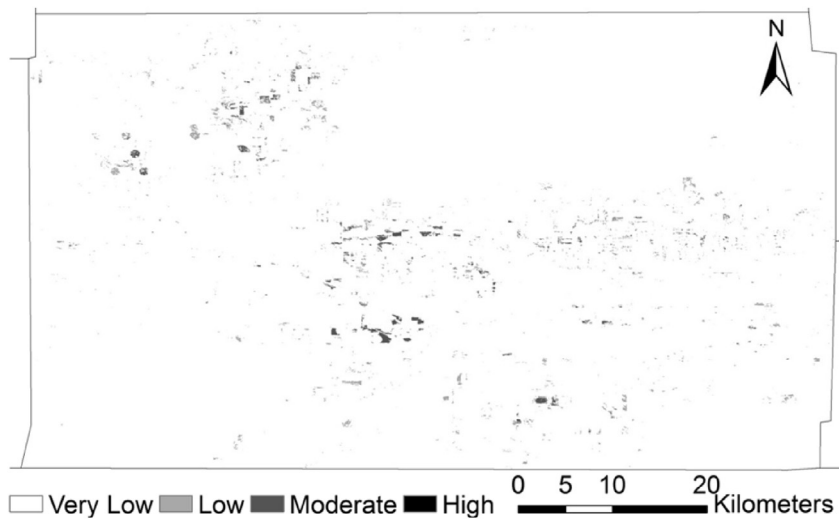


**Fig. 5.** Example of a risk map from hail events in 2010 produced for Cheyenne County, NE U.S.A. after using the normalized difference vegetation index as a crude land cover classification tool to separate wheat from surrounding vegetation.

actual risk. However, this remains to be examined due to limitations in data access.

While Landsat data was sufficient for most years, MODIS risk maps provided some additional coverage. Due to the more coarse spatial resolution, the MODIS maps averaged the risk in an area and extremes in scale were reduced. For example, there were fewer areas in the very low and high risk categories but a higher percentage of areas in the low and moderate risk categories. This suggests that improvements in accuracy for small target areas may

be possible when using higher spatial resolution four-band imagery, such as GeoEye, WorldView-2, SPOT or RapidEye.

While hail increased NIR reflectance, over time NIR reflectance decreased. Thus, the further the image was acquired from the actual hail event, the lower the level of risk that was assessed by the model. This means that some high risk areas will be underestimated. Inclusion of additional data sources may help resolve some temporal and spatial issues, but will increase processing time to produce the final map(s). Data fusion techniques may be

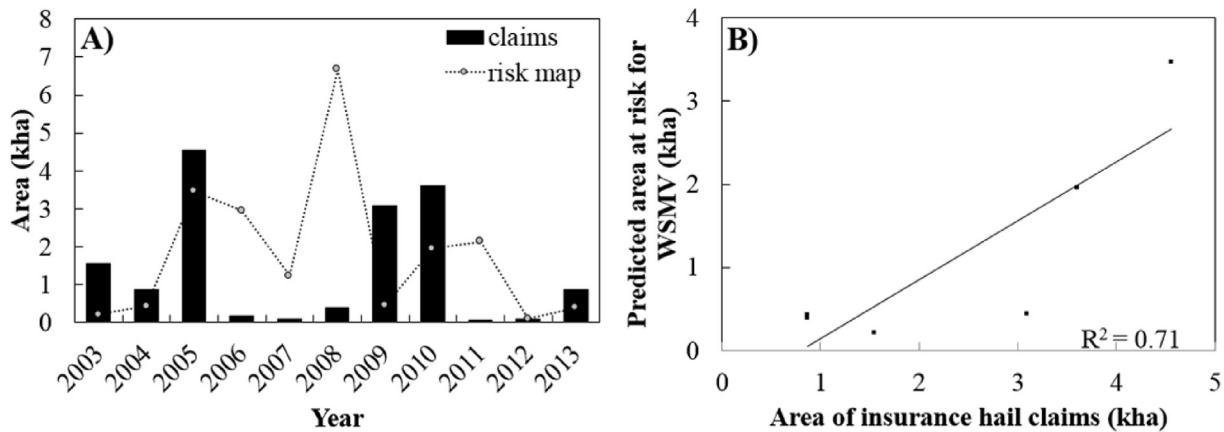


**Fig. 6.** Comparison of the risk maps with hail claims made during the integration of the NOAA hail product (Table 2): A) Area of hail claims and area identified as 'at risk' using the reflectance only products in Cheyenne County, NE, U.S.A. by year and B) the relationship between these two measurements for years when hail claims totaling less than 400 ha were excluded.

beneficial for timelier reflectance estimates; however, care must be taken to not remove the hail signature during processing. Costs and benefits, in addition to accuracy assessments, need to be fully examined before the model can be put into operation.

### 3.3. Potential improvements for the model

There were several weaknesses in the current model. Spatial and temporal resolution limited the current model. The increase in reflectance due to a hail event was fairly short-lived ( $\leq 7$  days); therefore, data with high temporal resolution was needed to catch all events. In addition, hail events tend to be localized in Nebraska. Data with high spatial resolution was also needed to identify risks at the field-level. It was expected that if spatial and temporal resolution of the inputs were low, risks would be underestimated. Utilizing alternative inputs, such as satellite imagery from newly launched sensors or unmanned aerial vehicles, may help improve the temporal and spatial resolution of reflectance data input into the model. There is potential for improved temporal resolution by including European Space Agency data as many Landsat-like products are being developed for Sentinel-2 (Zhu et al., 2015). Additionally, the spatial resolution of the NOAA hail product may not be fine enough to identify fields impacted by hail in isolated storms; however, minor improvements could be made using its high observation frequency. For example, the highest risk of volunteer wheat occurs when the wheat is mature. Early hail events could be classified at a lower risk than those that occur near harvest. However, this does increase the complexity of the model.

Secondly, the model does not identify fields where volunteer wheat was likely to occur. Identifying volunteer wheat growth or the potential for its growth would be beneficial. Identifying volunteer wheat was technically feasible using reflectance data; however, there are several problems with this approach. Volunteer wheat was generally localized, clumped, and stunted (Fig. 1: HD Post 14). It will be difficult to distinguish between pre-harvest volunteer wheat resulting from hail events and post-harvest volunteer wheat that poses less risk for virus transmission. These factors make it difficult to use reflectance for identifying volunteer wheat, especially for coarse data sets that may result in many mixed pixels. Alternatively, other elements that contributed to volunteer wheat growth could be included in the model. For example, the presence of dislodged grain increased the likelihood of producing volunteer wheat, but the grains themselves must germinate to pose a risk. Generally storms that bring hail provide

moisture needed for germination; however, it is not uncommon for the soil to dry rapidly after a rain event, reducing the likelihood of germination. Thus, incorporating local weather data may improve risk determination. Additionally, residue remaining after harvest can shelter dislodged grain and newly germinated volunteer wheat and prevent it from drying quickly. Since farmers may not harvest severely hailed fields, the increase in surface residue may help protect dislodged grains. Methods for estimating residue cover (Zheng et al., 2012) may also improve the risk model.

The maturity of the grain was another factor that impacted risk. Identification of the phenological stage at the hail event could improve the model through the assignment of different risk potential to different stages. Several remote sensing approaches have been developed for identifying phenological changes in wheat and other crops (Lu et al., 2013; Nguy-Robertson et al., 2013); however, the biggest limitation to incorporating these models was the spatial and temporal resolution necessary to produce accurate results. Some spatial limitations may be mitigated using a regional estimate if planting dates and maturity rates for the wheat crop in the area were similar. Temporal resolution issues can be mitigated, in part, by using interpolation techniques as phenology progresses at a predictable pace (Nguy-Robertson et al., 2013).

## 4. Conclusions

This study provided a conceptual framework for developing a risk map for wheat diseases caused by WCM-vectored viruses based on pre-harvest hail events. Traditional methods that use NDVI were found to be unsuitable due to low chlorophyll content in wheat at harvest. Hail events increased canopy albedo. While red reflectance increased during senescence, NIR reflectance typically decreased. Therefore, any increase in NIR combined with large increases in red reflectance over time can be used to assign some level of virus transmission risk due to hail damage. The model presented in this study utilized Landsat TM/ETM+ data due to necessary spatial resolution to resolve localized hail events commonly found in the Central Plains of the U.S.A. MODIS imagery was used to help gap-fill missing data due to cloud cover and the scan-line error in Landsat 7 imagery. The model was also supported by NOAA hail maps that estimated the size of hail that reached the ground in a given region. Once the size of the hail was known, a risk level was assigned. The final risk map was a combination of each of these individual risk products.

We examined the risk maps developed for one county,

Cheyenne County in Nebraska, and found that they roughly correlated to insurance claims from hail damage, thus providing support for the approach. However, there were some limitations in the method that need to be addressed before this product can become operational. First, the increase in albedo due to a hail event was fairly short-lived (<7 days); thus, timely imagery was necessary. While it could be technically feasible to use a data set with high temporal resolution, such as MODIS, spatial resolution was also a concern due to the localized nature of the hail events. These factors will result in an underestimation of risk. In contrast, overestimation will occur when fields other than wheat are included in the model. Accurate classification is necessary for the validation of the model.

Further research is needed to verify hail damage predicted by these maps in real-world situations. The biggest improvement in risk predictions would be derived from having data sets with high temporal and spatial resolution; however, this is unlikely to occur in the near-future. This risk map provides a level of risk for volunteer wheat to provide a summer “green bridge” for mites and virus; however, other environmental factors govern the extent of germination of grain shelled out by hail. Other improvements in these predictions could potentially be made by incorporating ancillary data such as weather and phenology to provide a level of risk due to the potential for volunteer wheat germination.

## Acknowledgements

This project was supported in part by funds provided through the United States Department of Agriculture, USDA-NIFA grant number 2013-68004-20358. We sincerely appreciate the support and the use of facilities and equipment provided by the Center for Advanced Land Management Information Technologies (CALMIT), School of Natural Resources and High Plains Ag Lab. We also thank the USDA-Risk Management Agency (Jeff Darrow, Topeka Office) for providing the aggregated county-level insurance claim data.

## References

- Bargiel, D., Herrmann, S., 2011. Multi-temporal land-cover classification of agricultural areas in two European regions with high resolution spotlight TerraSAR-X Data. *Remote Sens.* 3 (12), 859–877. <http://dx.doi.org/10.3390/rs3050859>.
- Burrows, M., Franc, G., Rush, C., Blunt, T., Ito, D., Kinzer, K., Olson, J., O'Mara, J., Price, J., Tande, C., Ziems, A., Stack, J., 2009. Occurrence of viruses in wheat in the Great Plains region. 2008. *Plant Health Prog.* <http://dx.doi.org/10.1094/PH-2009-0706-01-RS>.
- Byamukama, E., Seifers, D.L., Hein, G.L., De Wolf, E., Tisserat, N.A., Langham, M.A.C., Osborne, L.E., Timmerman, A., Wegulo, S.N., 2013. Occurrence and distribution of Triticum mosaic virus in the central Great Plains. *Plant Dis.* 97 (1), 21–29. <http://dx.doi.org/10.1094/PDIS-06-12-0535-RE>.
- Byamukama, E., Wegulo, S.N., Tatini, S., Hein, G.L., Graybosch, R.A., Baenziger, P.S., French, R., 2014. Quantification of yield loss caused by Triticum mosaic virus and wheat streak mosaic virus in winter wheat under field conditions. *Plant Dis.* 98 (1), 127–133. <http://dx.doi.org/10.1094/PDIS-04-13-0419-RE>.
- Cavanaugh, D.E., Schultz, J.A., 2012. WSR-88D signatures associated with one inch hail in the Southern Plains. *Electron. J. Oper. Meteorol.* 13 (1), 1–14.
- Changnon, S.A., 1971. Hailfall characteristics related to crop damage. *J. Appl. Meteorol.* 10 (2), 270–274. [http://dx.doi.org/10.1175/1520-0450\(1971\)010<0270:HCRICD>2.0.CO;2](http://dx.doi.org/10.1175/1520-0450(1971)010<0270:HCRICD>2.0.CO;2).
- Ellis, M.H., Rebetzke, G.J., Mago, R., Chu, P., 2003. First report of Wheat streak mosaic virus in Australia. *Australas Plant Pathol.* 32, 551–553.
- Erickson, B.J., Johannsen, C.J., Vorst, J.J., Biehl, L.L., 2004. Using remote sensing to assess stand loss and defoliation in Maize. *Photogramm. Eng. Remote Sens.* 70 (6), 717–722. <http://dx.doi.org/10.1080/PERS.70.6.717>.
- Gallo, K., Smith, T., Jungbluth, K., Schumacher, P., 2012. Hail swaths observed from satellite data and their relation to radar and surface-based observations: a case study from Iowa in 2009. *Weather Forecast.* 27 (3), 796–802. <http://dx.doi.org/10.1175/WAF-D-11-00118.1>.
- Gibson, W.W., Painter, R.H., 1956. The occurrence of wheat curl mites, *Aceria Tulipae* (K.), (Eriophyidae), a vector of wheat streak mosaic on winter wheat seedlings grown from infested kernels. *Trans. Kans. Acad. Sci.* (1903) 59 (4), 492. <http://dx.doi.org/10.2307/3626317>.
- Gitelson, A.A., 2011. Remote sensing estimation of crop biophysical characteristics at various scales. In: Thenkabail, P.S., Lyon, J.G., Huete, A.R. (Eds.), *Hyperspectral Remote Sensing of Vegetation*. Taylor and Francis, pp. 329–358.
- Gosling, P.G., Butler, R.A., Black, M., Chapman, J.M., 1981. The onset of germination ability in developing wheat. *J. Exp. Bot.* 32 (3), 621–627. <http://dx.doi.org/10.1093/jxb/32.3.621>.
- Huth, J., Kuenzer, C., Wehrmann, T., Gebhardt, S., Tuan, V.Q., Dech, S., 2012. Land cover and land use classification with TWOPAC: towards automated processing for pixel- and object-based image classification. *Remote Sens.* 4 (12), 2530–2553. <http://dx.doi.org/10.3390/rs4092530>.
- Irish, R.R., Barker, J.L., Goward, S.N., Arvidson, T., 2006. Characterization of the Landsat-7 ETM+ automated cloud-cover assessment (ACCA) algorithm. *Photogramm. Eng. Remote Sens.* 72 (10), 1179–1188.
- Jackson, R.D., Teillet, P.M., Slater, P.N., Fedosejevs, G., Jasinski, M.F., Aase, J.K., Moran, M.S., 1990. Bidirectional measurements of surface reflectance for view angle corrections of oblique imagery. *Remote Sens. Environ.* 32, 189–202. [http://dx.doi.org/10.1016/0034-4257\(90\)90017-G](http://dx.doi.org/10.1016/0034-4257(90)90017-G).
- Jedlovec, G.J., Nair, U., Haines, S.L., 2006. Detection of storm damage tracks with EOS data. *Weather Forecast.* 21 (3), 249–267. <http://dx.doi.org/10.1175/WAF923.1>.
- Kalb, D., Bentley, M.L., 2002. Using Landsat to identify thunderstorm damage in agricultural regions. *Bull. Am. Meteorol. Soc.* 83 (3), 363–376.
- Lakshmanan, V., Smith, T., Stumpf, G.J., Hondl, K., 2007. The warning decision support system – integrated information (WDSS-II). *Weather Forecast.* 22, 596–612.
- Lu, L., Wang, C., Guo, H., Li, Q., 2013. Detecting winter wheat phenology with SPOT-VEGETATION data in the North China Plain. *Geocarto Int.* 29 (3), 244–255. <http://dx.doi.org/10.1080/10106049.2012.760004>.
- Maiersperger, T.K., Scaramuzza, P.L., Leigh, L., Shrestha, S., Gallo, K.P., Jenkerson, C.B., Dwyer, J.L., 2013. Characterizing LEDAPS surface reflectance products by comparisons with AERONET, field spectrometer, and MODIS data. *Remote Sens. Environ.* 136, 1–13. <http://dx.doi.org/10.1016/j.rse.2013.04.007>.
- Masek, J.G., Vermote, E.F., Saleous, N.E., Wolfe, R., Hall, F.G., Huemmrich, K.F., Gao, F., Kutler, J., Lim, T.-K., 2006. A Landsat surface reflectance dataset for North America, 1990–2000. *IEEE Geosci. Remote Sens. Lett.* 3 (1), 68–72. <http://dx.doi.org/10.1109/LGRS.2005.857030>.
- Maxwell, S.K., Schmidt, G.L., Storey, J.C., 2007. A multi-scale segmentation approach to filling gaps in Landsat ETM+ SLC-off images. *Int. J. Remote Sens.* 28 (23), 5339–5356. <http://dx.doi.org/10.1080/01431160601034902>.
- Molthan, A.L., Burks, J.E., Mcgrath, K.M., Lafontaine, F.J., 2013. Multi-sensor examination of hail damage swaths for near real-time applications and assessment, 1 (13), 144–156.
- Nebraska Department of Agriculture, 2012. Nebraska Agriculture, p. 31. Lincoln, NE. Retrieved from. [http://www.nda.nebraska.gov/publications/ne\\_ag\\_facts\\_brochure.pdf](http://www.nda.nebraska.gov/publications/ne_ag_facts_brochure.pdf).
- Nguy-Robertson, A.L., Gitelson, A.A., Peng, Y., Walter-Shea, E.A., Leavitt, B., Arkebauer, T.J., 2013. Continuous monitoring of crop reflectance, vegetation fraction and identification of developmental stages using a four band radiometer. *Agron. J.* 105 (6), 1769. <http://dx.doi.org/10.2134/agronj2013.0242>.
- Ortega, K.L., Smith, T.M., Manross, K.L., Scharfenberg, K.A., Witt, A., Kolodziej, A.G., Gourley, J.J., 2009. The severe hazards analysis and verification experiment. *Bull. Am. Meteorol. Soc.* 90, 1519–1530.
- Parker, M.D., Ratcliffe, I.C., Henebry, G.M., 2005. The July 2003 Dakota hailswaths: creation, characteristics, and possible impacts. *Mon. Weather Rev.* 133 (5), 1241–1261.
- Peters, A.J., Griffin, S.C., Viña, A., Ji, L., 2000. Use of remotely sensed data for assessing crop hail damage. *Photogramm. Eng. Remote Sens.* 66 (11), 1349–1355.
- R Development Core Team, 2015. R: A Language and Environment for Statistical Computing. R Foundation for Statistical Computing, Vienna, Austria, ISBN 3-900051-07-0. <http://www.R-project.org>.
- Robertson, L.D., Curtis, B.C., 1967. Germination of immature kernels of winter wheat. *Crop Sci.* 7 (3), 269. <http://dx.doi.org/10.2135/cropsci1967.0011183X000700030033x>.
- Rundquist, D.C., Perk, R., Leavitt, B., Keydan, G.P., Gitelson, A.A., 2004. Collecting spectral data over cropland vegetation using machine-positioning versus hand-positioning of the sensor. *Comput. Electron. Agric.* 43 (2), 173–178. <http://dx.doi.org/10.1016/j.compag.2003.11.002>.
- Sánchez, J.L., Fraile, R., de la Madrid, J.L., de la Fuente, M.T., Rodríguez, P., Castro, A., 1996. Crop damage: the hail size factor. *J. Appl. Meteorol.* 35 (9), 1535–1541. [http://dx.doi.org/10.1175/1520-0450\(1996\)035<1535:CDTHSF>2.0.CO;2](http://dx.doi.org/10.1175/1520-0450(1996)035<1535:CDTHSF>2.0.CO;2).
- Schiesser, H.H., Backfile, P.S., 1990. Hailfall: the relationship between radar measurements and crop damage. *Atmos. Res.* 25 (6), 559–582. [http://dx.doi.org/10.1016/0169-8095\(90\)90038-E](http://dx.doi.org/10.1016/0169-8095(90)90038-E).
- Schubert, J., Ziegler, A., Rabenstein, F., 2015. First detection of wheat streak mosaic virus in Germany: molecular and biological characteristics. *Arch. Virol.* 160 (7), 1761–1766. <http://dx.doi.org/10.1007/s00705-015-2422-2>.
- Seifers, D.L., Martin, T.J., Harvey, T.L., Fellers, J.P., Michaud, J.P., 2009. Identification of the wheat curl mite as the vector of triticum mosaic virus. *Plant Dis.* 93 (1), 25–29. <http://dx.doi.org/10.1094/PDIS-93-1-0025>.
- Seifers, D.L., Martin, T.J., Harvey, T.L., Haber, S., 2007. Temperature-sensitive *Wheat streak mosaic virus* resistance identified in KS03HW12 wheat. *Plant Dis.* 91 (8). <http://dx.doi.org/10.1094/PDIS-91-8-1029>.
- Shahwan, I.M., Hill, J.P., 1984. Identification and occurrence of wheat Streak Mosaic Virus in winter wheat in Colorado and its effects on several wheat cultivars. *Plant Dis.* 68 (7), 579. <http://dx.doi.org/10.1094/PD-69-579>.
- Slykhuus, J.T., 1955. *Aceria tulipae* Keifer (Acarina: Eriophyidae) in relation to the spread of wheat streak mosaic. *Phytopathology* 45, 116–128.
- Smith, T.M., Lakshmanan, V., 2011. Real-time, rapidly updating severe weather

- products for virtual globes. *Comput. Geosci.* 37, 3–12. Virtual Globes in Science special issue.
- Somsen, H.W., Sill, W.H., 1970. The Wheat Curl Mite, *Aceria Tulipae* Keifer, in Relation to Epidemiology and Control of Wheat Streak Mosaic by (No. Research Publication 162), p. 24 (Manhattan, KS).
- Starks, P.J., Steiner, J.L., Stern, A.J., 2014. Upper Washita River experimental watersheds: land cover data sets (1974–2007) for two Southwestern Oklahoma agricultural watersheds. *J. Environ. Qual.* 43 (4), 1310–1318. <http://dx.doi.org/10.2134/jeq2013.07.0292>. July 2013.
- Tatineni, S., Ziems, A.D., Wegulo, S.N., French, R., 2009. *Triticum mosaic virus*: a distinct member of the family *Potyviridae* with an unusually long leader sequence. *Phytopathology* 99, 943–950.
- Thomas, J.A., Hein, G.L., Lyon, D.J., 2004. Spread of wheat curl mite and wheat streak mosaic virus is influenced by volunteer wheat control methods. *Plant Health Prog.* <http://dx.doi.org/10.1094/PHP-2004-1206-01-RS>. December.
- Truol, G., French, R., Sagadin, M., Arneodo, J., 2004. First report of Wheat streak mosaic virus infecting wheat in Argentina. *Aust. Plant Pathol.* 33, 137–138.
- Tucker, C.J., 1979. Red and photographic infrared linear combinations for monitoring vegetation. *Remote Sens. Environ.* 8 (2), 127–150. [http://dx.doi.org/10.1016/0034-4257\(79\)90013-0](http://dx.doi.org/10.1016/0034-4257(79)90013-0).
- Van Meter, J., Schueth, J., Pratt, K., Mills, C., 2012. Animal and Plant Health Protection Entomology Program 2012 Annual Report (No. Annual2012\_042213), p. 11. Lincoln, NE. Retrieved from [http://www.nda.nebraska.gov/plant/2012\\_entomology\\_annual\\_report.pdf](http://www.nda.nebraska.gov/plant/2012_entomology_annual_report.pdf).
- Vermote, E., Kotchenova, S., 2011. MODIS directional surface reflectance product: method, error estimates and validation. In: Ramachandran, B., Justice, C.O., Abrams, M.J. (Eds.), *Land Remote Sensing and Global Environmental Change*. Springer Science+Business Media, LLC, New York, NY, pp. 533–547. [http://dx.doi.org/10.1007/978-1-4419-6749-7\\_23](http://dx.doi.org/10.1007/978-1-4419-6749-7_23).
- Viña, A., Gitelson, A.A., Nguy-Robertson, A.L., Peng, Y., 2011. Comparison of different vegetation indices for the remote assessment of green leaf area index of crops. *Remote Sens. Environ.* 115 (12), 3468–3478. <http://dx.doi.org/10.1016/j.rse.2011.08.010>.
- Wardlow, B.D., Egbert, S., Kastens, J., 2007. Analysis of time-series MODIS 250 m vegetation index data for crop classification in the U.S. Central Great Plains. *Remote Sens. Environ.* 108 (3), 290–310. <http://dx.doi.org/10.1016/j.rse.2006.11.021>.
- Wosula, E.N., McMechan, A.J., Hein, G.L., 2015. The effect of temperature, relative humidity, and virus infection status on off-host survival of the wheat curl mite (*Acari: Eriophyidae*). *J. Econ. Entomol.* 108 (4), 1545–1552.
- Yuan, M., Dickens-Micozzi, M., Magsig, M.A., 2002. Analysis of tornado damage tracks from the 3 May tornado outbreak using multispectral satellite imagery. *Weather Forecast.* 17 (3), 382–398. [http://dx.doi.org/10.1175/1520-0434\(2002\)017.<0382:AOTDTF>2.0.CO;2](http://dx.doi.org/10.1175/1520-0434(2002)017.<0382:AOTDTF>2.0.CO;2).
- Zhang, C., Li, W., Travis, D., 2007. Gaps-fill of SLC-off Landsat ETM+ satellite image using a geostatistical approach. *Int. J. Remote Sens.* 28 (22), 5103–5122. <http://dx.doi.org/10.1080/01431160701250416>.
- Zhao, J.L., Zhang, D.Y., Luo, J.H., Huang, S.L., Dong, Y.Y., Huang, W.J., 2012. Detection and mapping of hail damage to corn using domestic remotely sensed data in China. *Aust. J. Crop Sci.* 6 (1), 101–108. [http://www.cropl.com/zhao\\_6\\_1\\_2012\\_101\\_108.pdf](http://www.cropl.com/zhao_6_1_2012_101_108.pdf).
- Zheng, B., Campbell, J.B., de Beurs, K.M., 2012. Remote sensing of crop residue cover using multi-temporal Landsat imagery. *Remote Sens. Environ.* 117, 177–183. <http://dx.doi.org/10.1016/j.rse.2011.09.016>.
- Zhu, Z., Wang, S., Woodcock, C.E., 2015. Improvement and expansion of the Fmask algorithm: cloud, cloud shadow, and snow detection for Landsats 4–7, 8, and Sentinel 2 images. *Remote Sens. Environ.* 159, 269–277. <http://dx.doi.org/10.1016/j.rse.2014.12.014>.